NARROWBAND GYROSYNCHROTRON BURSTS: PROBING ELECTRON ACCELERATION IN SOLAR FLARES

Gregory D. Fleishman, Gelu M. Nita*,
Eduard P. Kontar, and Dale E. Gary

(ApJ, 826 , 20 July 2016)

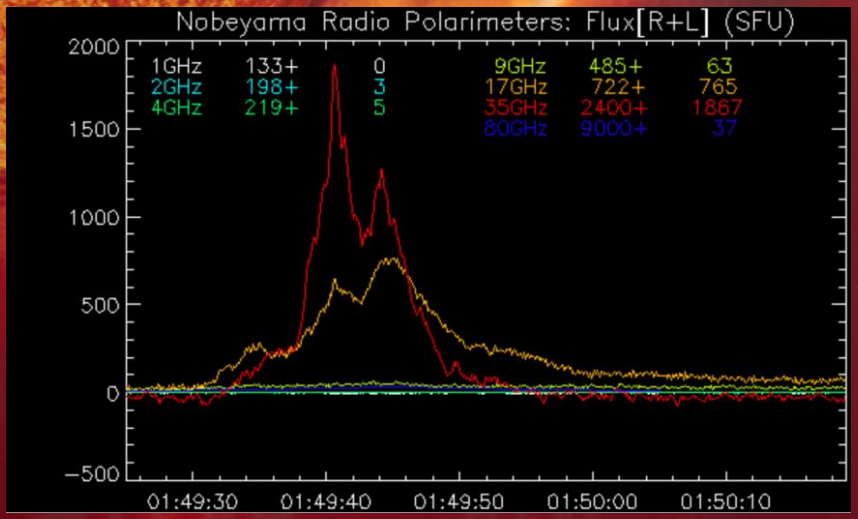

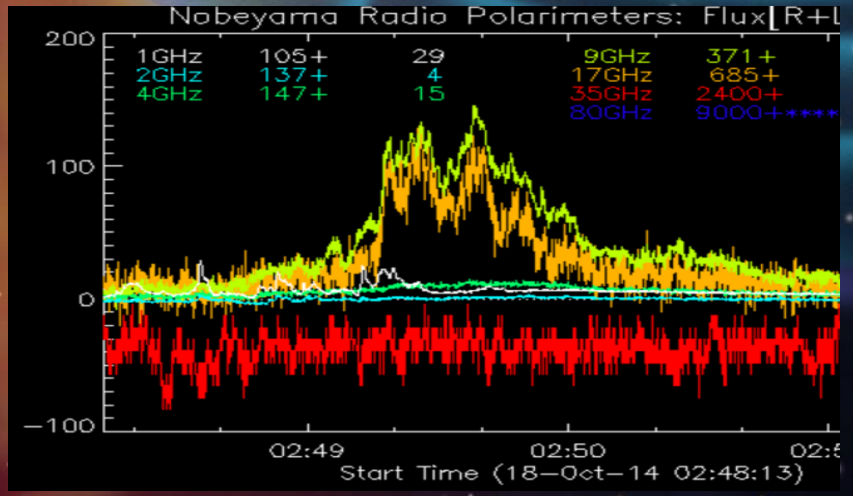

OVSA NARROWBAND BURSTS

$$|\delta_{lf,hf}| \geq 3$$

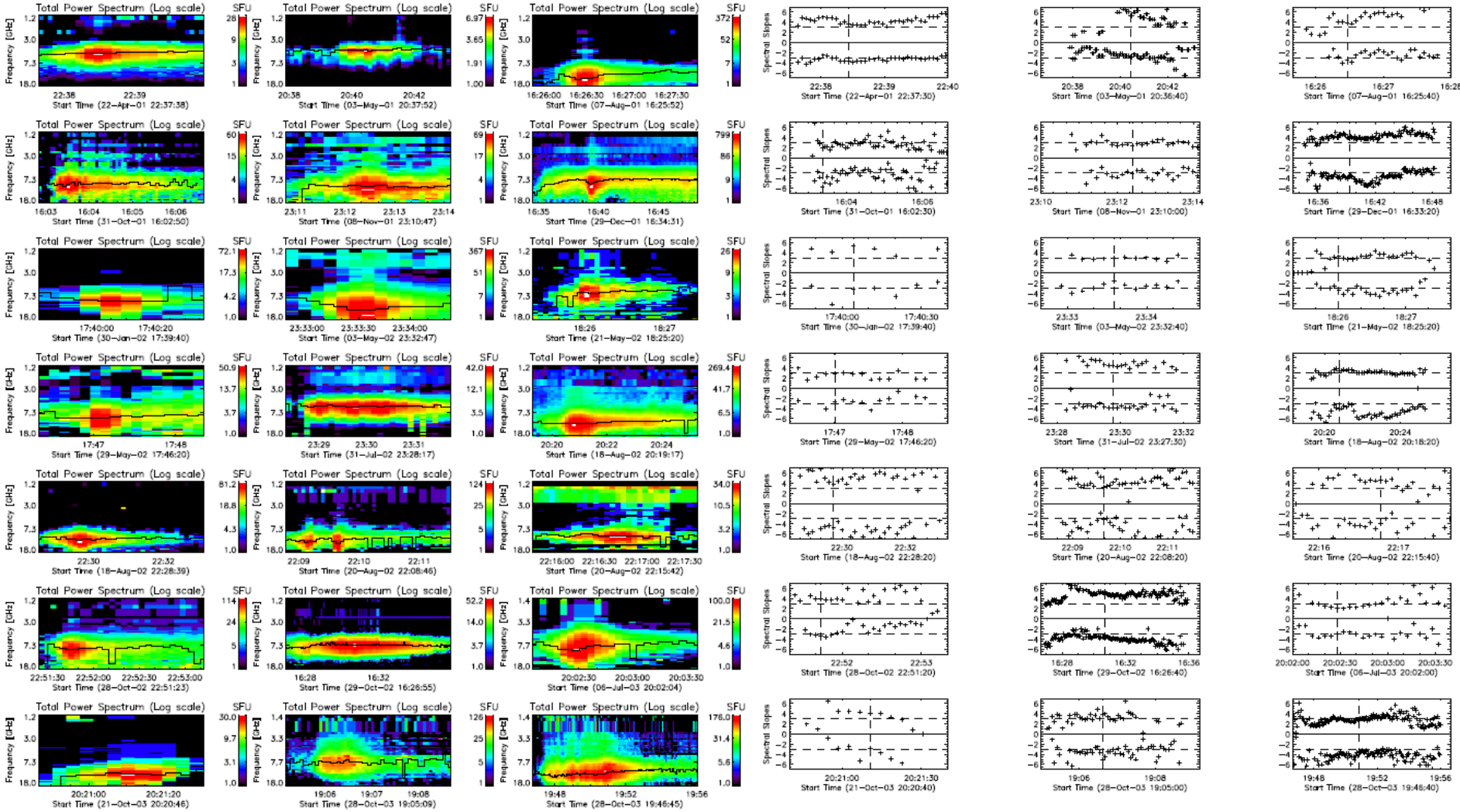

RHESSI and Microwave Images

6-9 keV; 9-15 keV; 25-50 keV

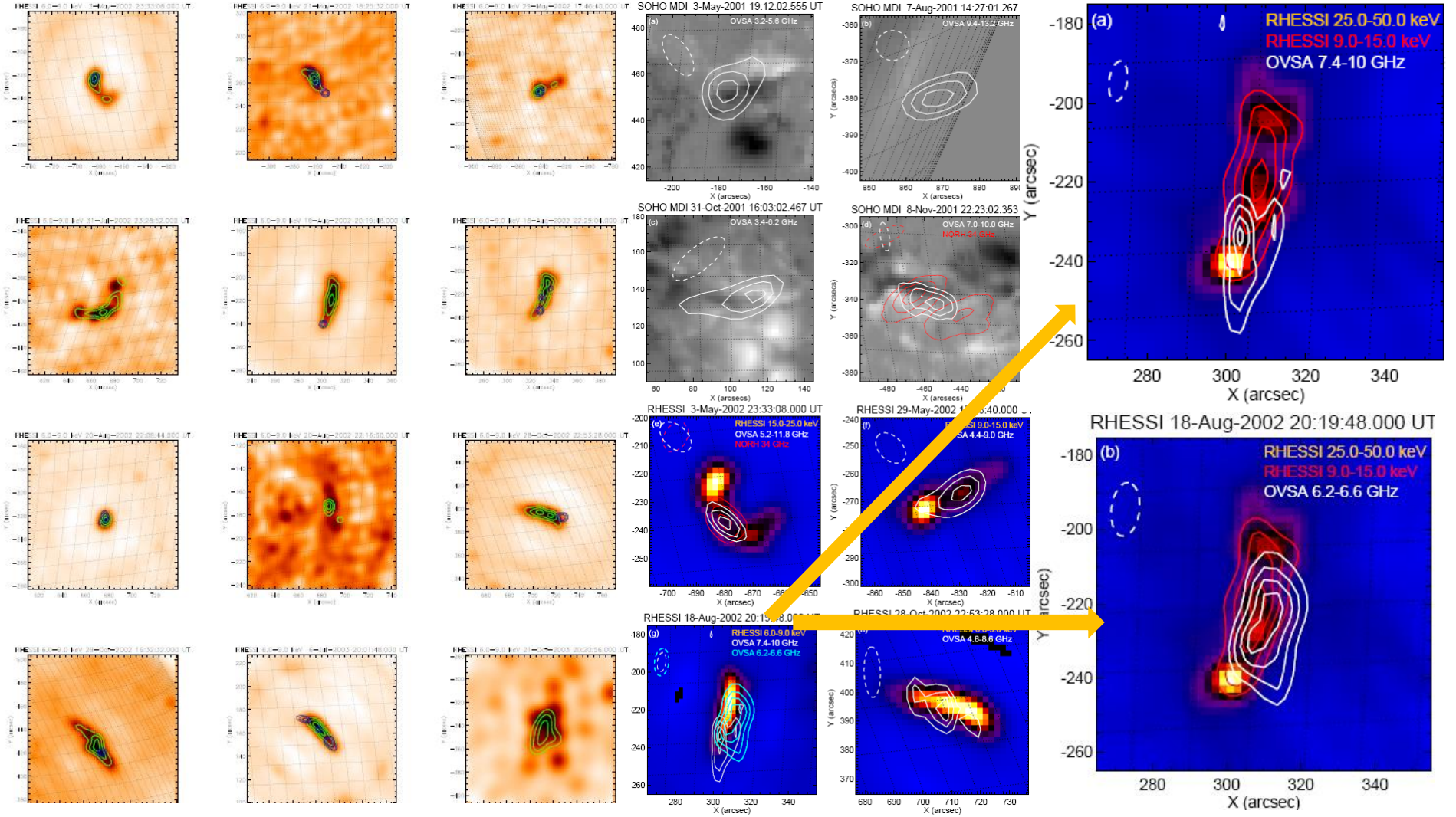

Acceleration & Trapping

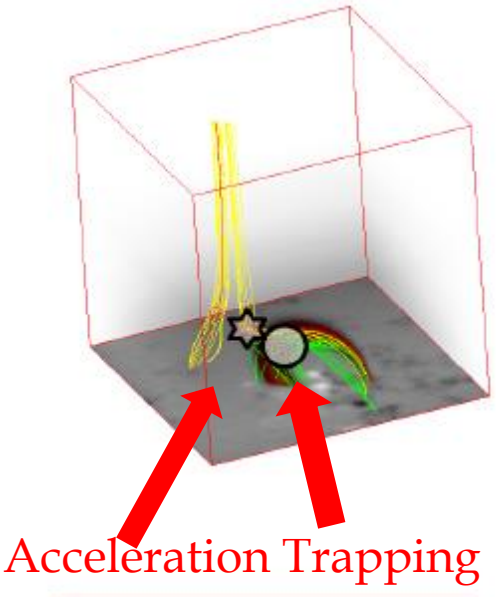

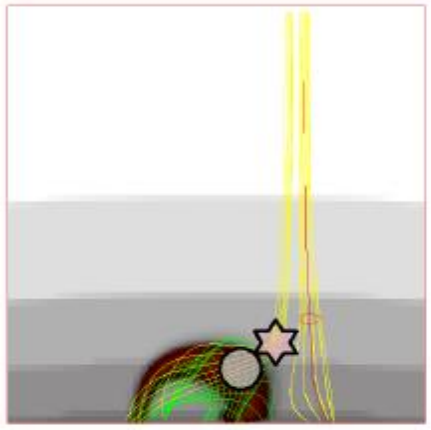

- A steep low-frequency spectrum implies that the emission is nonthermal, and the source is reasonably dense and uniform.
- A steep high-frequency spectrum implies that no significant electron trapping occurs, otherwise a progressive spectral flattening would be observed
- Based on an analysis of **radio-to-X-ray spatial relationships**, **timing**, and **spectral fits**, we concluded that the microwave emission in these narrowband bursts originates directly from the acceleration regions, which have a relatively strong magnetic field, high density, and low temperature.
- In contrast, the thermal X-ray emission comes from a distinct loop with a smaller magnetic field, lower density, but higher temperature.
- Therefore, these flares likely occurred due to interaction between two (or more) magnetic loops.

(Modeling performed in GX Simulator, Nita et al. 2015)

GS continuum radio emission can be the result of:

(i) a magnetically trapped component, or

(ii) a precipitating/escaping component, or

(iii) the primary component within the acceleration region.

These three populations of fast electrons produce ***radio emission with distinctly different*** characteristics:

(i) in the case of ***trapping*** the electrons are accumulated at the looptop (Melnikov et al. 2002), and the ***radio light curves must be delayed*** by roughly the trapping time relative to accelerator/X-ray light curves.

(ii) In the case of free electron propagation, untrapped precipitating electrons are more evenly distributed in a tenuous loop, and ***no delay*** longer than L/v is expected. However, even with a roughly uniform electron distribution, most of the radio emission comes from loop regions with the strongest magnetic field. **Spectral indices of the radio- and X-ray- producing fast electrons differ by 1/2 from each other**.

(iii) In the case of **radio emission from the acceleration region**, even though the residence time that fast electrons spent in the acceleration region can be relatively long, the ***radio and (thick-target, footpoint) X-ray light curves are proportional to each other*** simply because the flux of the X-ray producing electrons is equivalent to the electron loss rate from the acceleration region.

GS Spectral Fit Example: 2002-Apr-11

Fleishman et al. ApJ, 768, 2013

Emission from:

Acceleration region

Precipitating electrons

Trapped component

Microwave emission from the acceleration region can be very "narrowband", which implies a reasonable uniformity of the source

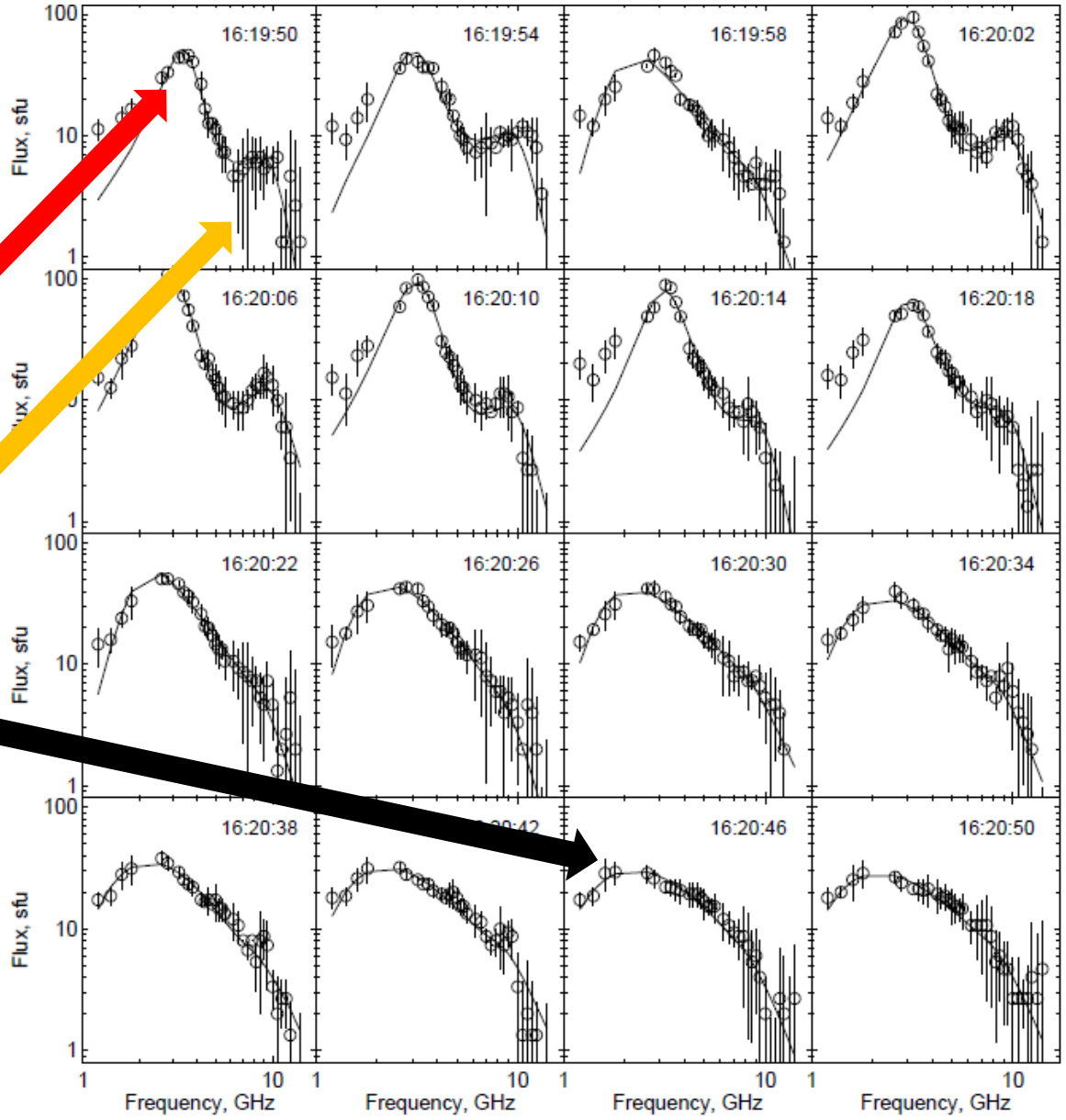

Example of source parameters that may be derived from spectral fit using GS fast codes
Fleishman and Kuznetsov, ApJ, 721, 2010

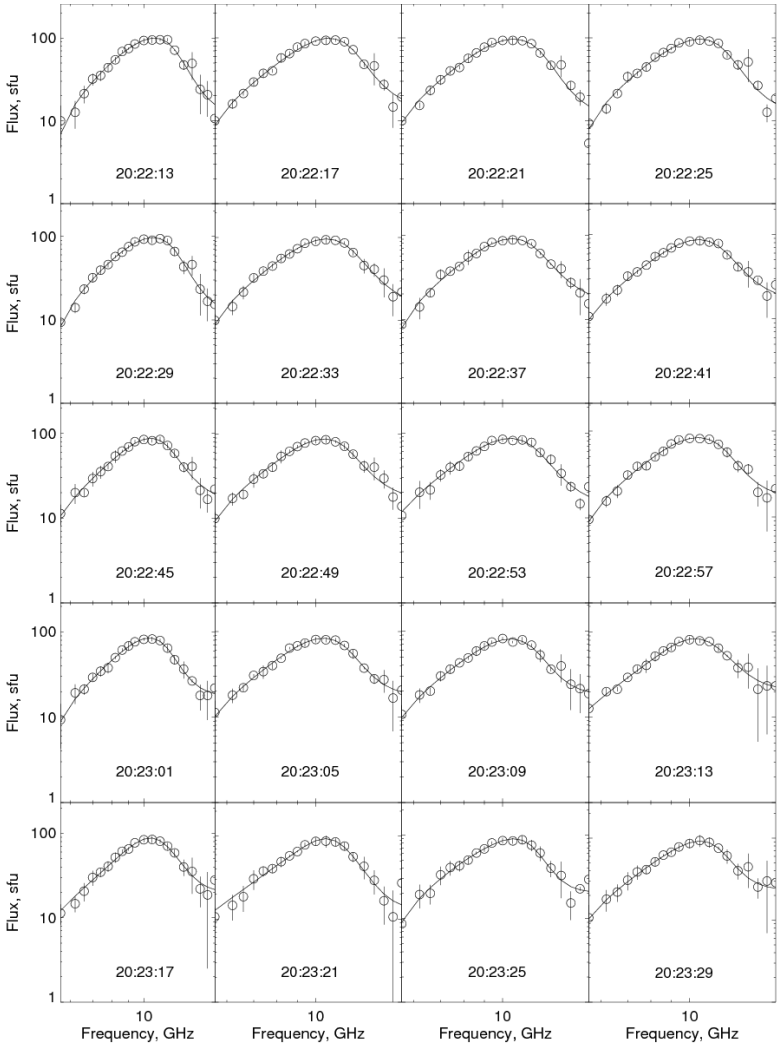

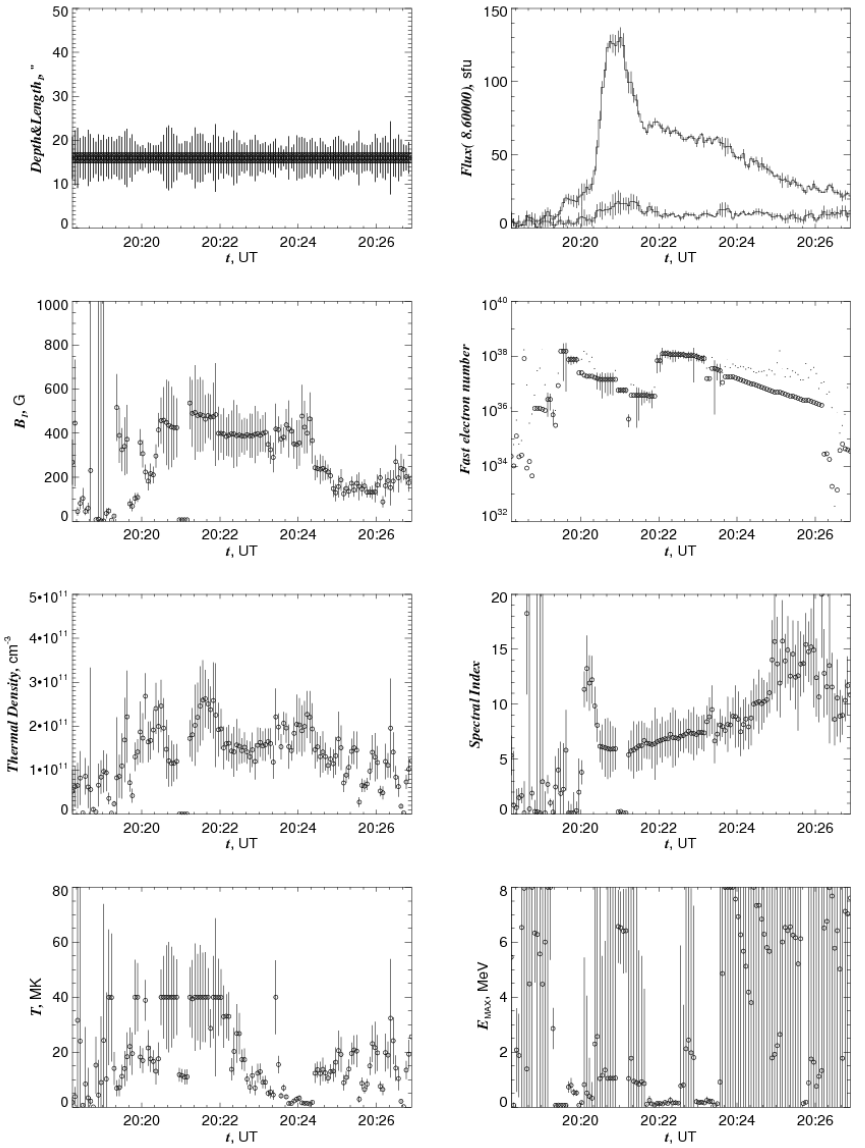

Fitting examples of spatially integrated X-ray spectrum

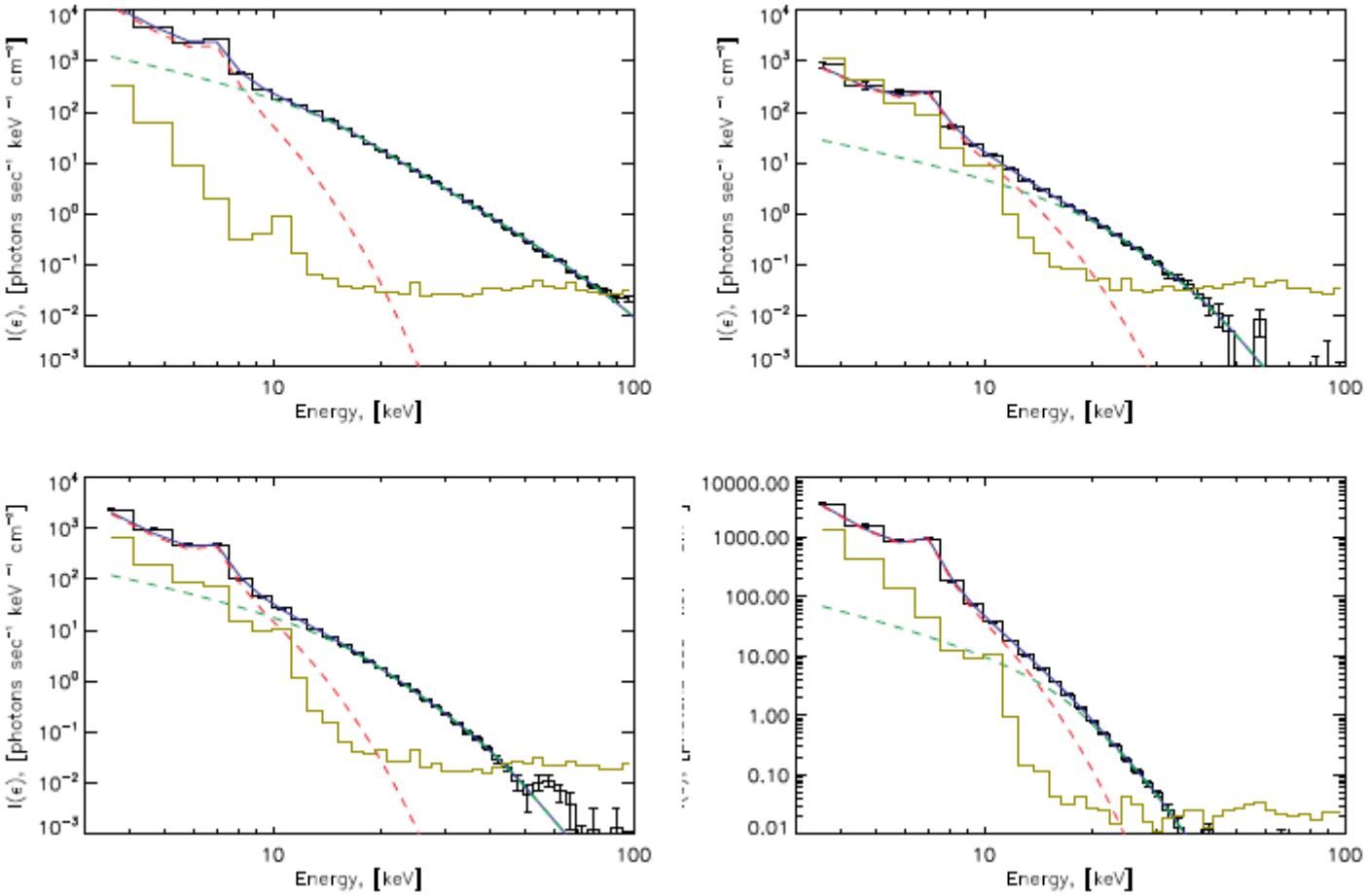

Flare parameters derived from fitting of spatially integrated X-ray spectrum

Flare	A_{6-9keV}	$A_{9-15keV}$	$\frac{EM}{10^{49}\ \mathrm{cm}^{-3}}$	T, MK	$\frac{N_e}{10^{35}\ \mathrm{s}^{-1}}$	E_{min}, keV	$\delta_{nth,X}$
03-May-2002 23:32	120	176	0.016	18.1	7.31	17.5	5.1
21-May-2002 18:25	172	176	0.0007	26	0.12	22.3	4.7
29-May-2002 17:46	92	116	0.0023	20.9	0.7	18.2	5.1
31-Jul-2002 23:27	328	468	0.0036	23.3	0.42	18.6	6.0
18-Aug-2002 20:18	260	360	0.15	17.1	20	14.8	7.3
18-Aug-2002 22:28	228	380	0.027	20.3	2.5	17.8	7.3
20-Aug-2002 22:08	76	92	0.011	21.6	0.8	17.7	6.1
20-Aug-2002 22:15	184	136	0.0001	30.2	0.016	21.8	4.9
28-Oct-2002 22:51	248	276	0.016	12.2	0.5	13.4	10.3
29-Oct-2002 16:26	396	388	0.14	20.6	0.87	21.1	10.0
06-Jul-2003 20:02	212	280	0.015	15.2	3.41	15.8	6.4
21-Oct-2003 20:20	580	676	0.0087	19.7	0.058	21.8	4.48

Flare parameters derived from microwave fit

Flare	sizes	B, G	$\left(\frac{n_{th}}{10^{11}\ \mathrm{cm}^{-3}}\right)^{\star}$	$\delta_{nth,r}$	$\frac{N_e}{10^{35}}$	T, MK
22-Apr-2001 2[illegible]:37†	$10'' \times 20''$	300 ± 50	0.7 ± 0.2	5 ± 1	0.2 ± 0.1	...
03-May-2001 2[illegible]:36	[illegible]	[illegible]	[illegible]	[illegible]	[illegible]	± 2
07-Aug-2001 1[illegible]:25	[illegible]	[illegible]	[illegible]	[illegible]	[illegible]	...
31-Oct-2001 1[illegible]:02	$15'' \times 30''$	300 ± 100	1.2 ± 0.2	8 ± 2	$1 - 10$	20 ± 5
08-Nov-2001 23:10	$10'' \times 25''$	$200 - 400$	1.5 ± 0.5	$6 - 9$	~ 10	10 ± 5
29-Dec-2001 16:33†	$20'' \times 40''$	350 ± 50	1 ± 0.5	$5 - 8$	$10 - 100$	...
30-Jan-2002 17:39†	$8'' \times 18''$	350 ± 100	1.5 ± 0.5	6 ± 1	~ 80	...
03-May-2002 23:32	$10'' \times 40''$	550 ± 100	1.5 ± 0.5 (0.1)	5 ± 1	~ 10	...
21-May-2002 18:25‡	$10'' \times 20''$	270 ± 70	0.3 ± 0.1 (0.03)	7.5 ± 1.5	$1 - 3$	$5 - 10$
29-May-2002 17:46	$10'' \times 20''$	400 ± 100	$0.5 - 1.5^{\Uparrow}$ (0.05)	7 ± 1	$0.1 - 1$	$5 - 20^{\Uparrow}$
31-Jul-2002 23:27‡	$10'' \times 30''$	350 ± 100	0.8 ± 0.4 (0.055)	7 ± 2	$0.1 - 3$	...
18-Aug-2002 20:18	$10'' \times 30''$	400 ± 100	1.5 ± 0.5 (0.35)	6 ± 1	~ 20	...
18-Aug-2002 22:28‡	$10'' \times 30''$	$200 - 500$	$1 - 2$ (0.15)	> 7	$1 - 10$	...
20-Aug-2002 22:08‡	$10'' \times 12''$	500 ± 100	0.7 ± 0.3 (0.15)	7 ± 2	5 ± 3	...
20-Aug-2002 22:15‡	$10'' \times 12''$	600 ± 100	1.2 ± 0.3 (0.015)	7 ± 2	$0.1 - 3$	...
28-Oct-2002 22:51	$10'' \times 30''$	500 ± 100	1.5 ± 0.5 (0.12)	5 ± 1	$0.01 - 0.8$	...
29-Oct-2002 16:26‡	$10'' \times 20''$	470 ± 70	1.2 ± 0.2 (0.4)	$5 \pm 1^{\sharp}$	$0.1 - 0.3$	...
06-Jul-2003 20:02‡	$11'' \times 25''$	350 ± 100	0.6 ± 0.1 (0.11)	5 ± 1	$1 - 10$	20 ± 10
21-Oct-2003 20:20‡	$10'' \times 30''$	400 ± 100	3 ± 1 (0.085)	8 ± 2	~ 1	7 ± 3
28-Oct-2003 19:05†	variable	$300 - 800$	$0.1 - 2^{\Uparrow}$	> 5	$0.1 - 1$	$1 - 15^{\Uparrow}$
28-Oct-2003 19:46†	$10'' \times 20''$	$500 - 1000^{\cup}$	2 ± 1	$5 \pm 1^{\cap\sharp}$	$0.3 - 5$	...

Densities derived from MW fits are systematically much higher than those derived from X-ray fits

FREQUENCY-DEPENDENT TIME DELAYS

Cold dense flare;
Bastian et al. 2007

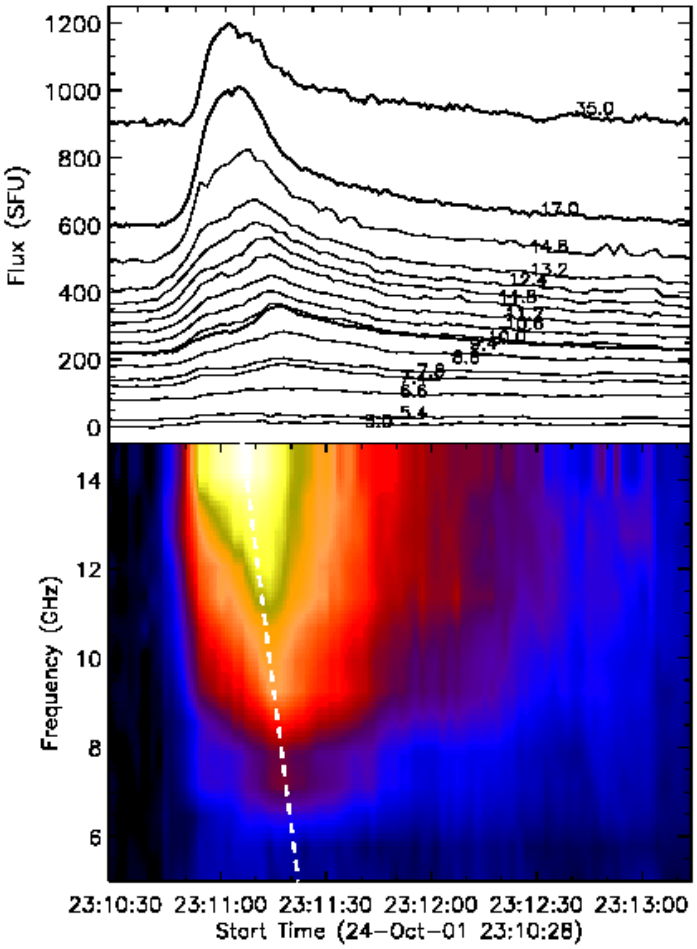

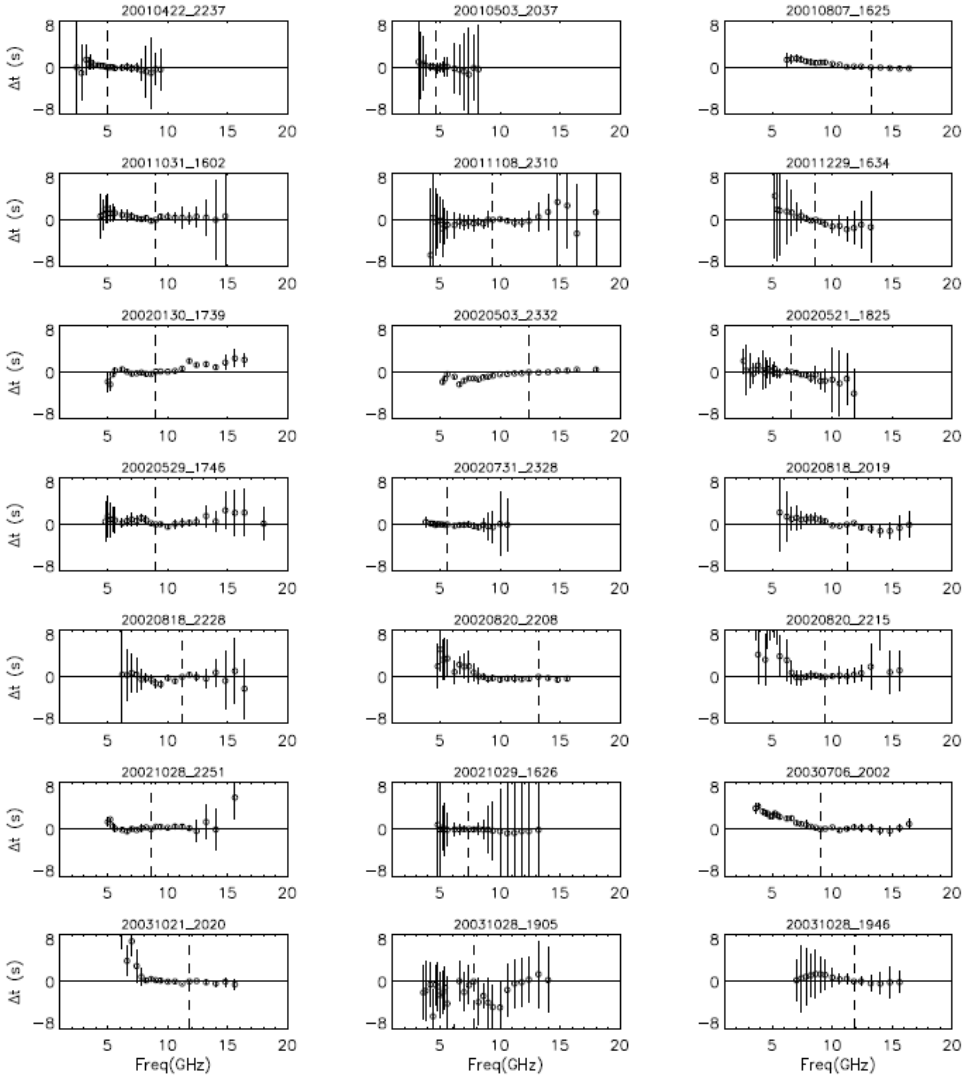

Trapping regimes

Theoretically expected power index of the frequency-dependent decay constants for different trapping regimes

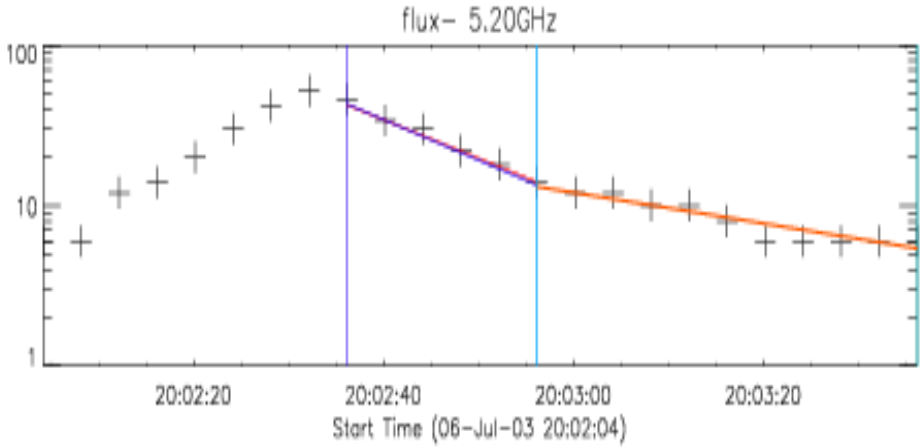

$$I = I_0 \exp\left[-\frac{t}{\tau(f)}\right]$$

$$\tau(f) \sim f^{\delta_{1,2}}$$

(1) Regime	(2) $\tau(E)$; nonrel.	(3) δ; nonrel	(4) Range of δ	(5) $\tau(E)$; rel.	(6) δ; rel	(7) Range of δ
Weak diff.; Coulomb	$E^{3/2}$	$\frac{3}{2a}$	$1 < \delta < 3/2$	E^{1}	$1/2$	$1/2$
Weak diff.; Turb.	$E^{(1-\nu)/2}$	$\frac{1-\nu}{2a}$	$-\frac{1}{2} < \delta < 0$	$E^{(2-\nu)}$	$\frac{2-\nu}{2}$	$0 < \delta < \frac{1}{2}$
Moderate diffusion	$E^{-1/2}$	$-\frac{1}{2a}$	$-1/2 < \delta < -1/3$	E^{0}	0	0
Strong diffusion	$E^{(\nu-3)/2}$	$\frac{\nu-3}{2a}$	$-1 < \delta < -\frac{1}{3}$	$E^{(\nu-2)}$	$\frac{\nu-2}{2}$	$-\frac{1}{2} < \delta < 0$

FREQUENCY-DEPENDENT TIME DECAY CONSTANTS

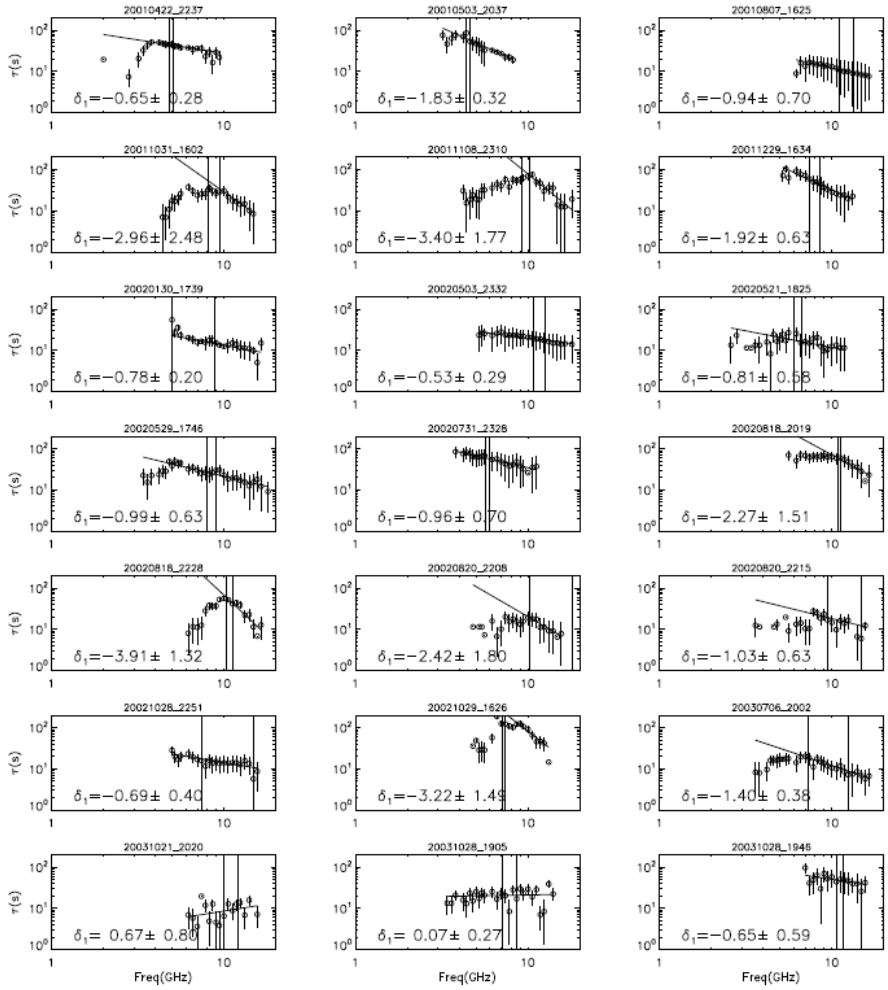

$$\tau(f) \propto f^{\delta_1}$$

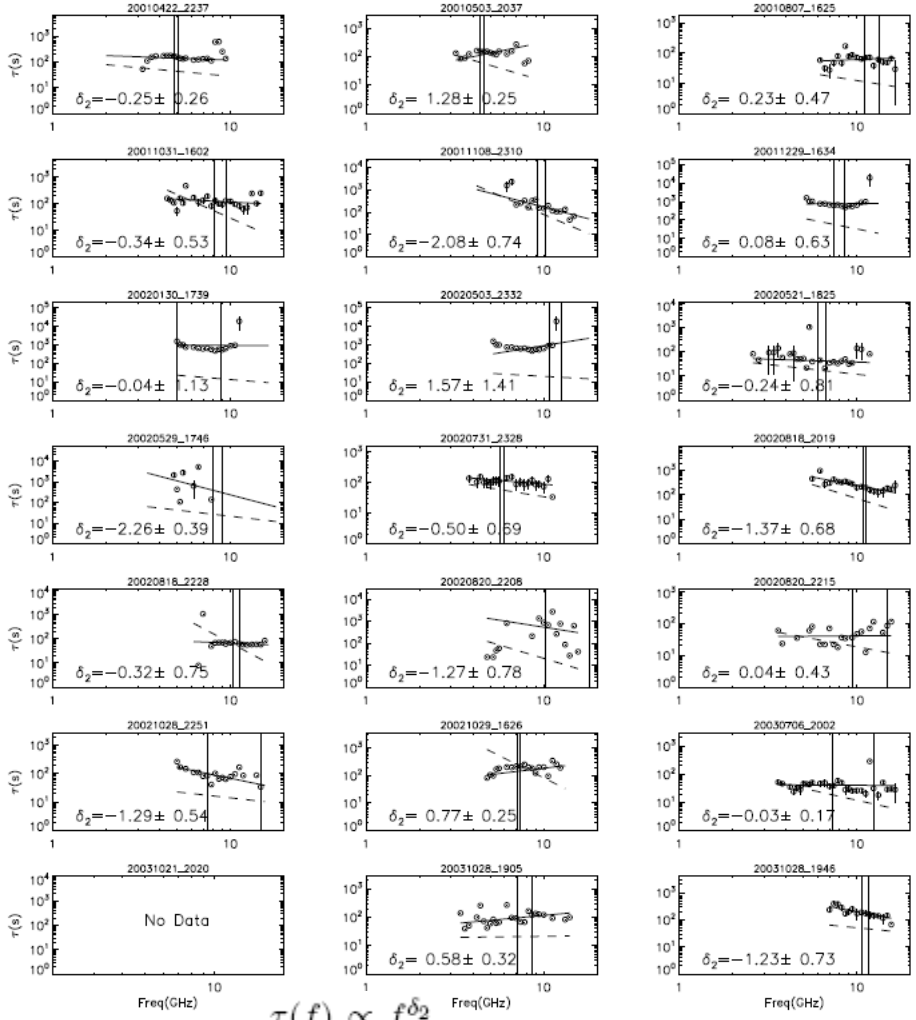

$$\tau(f) \propto f^{\delta_2}$$

Interpretation of timing and spectral evolution

- These events display no significant trapping of the fast electrons at the main phases of the bursts, rather **microwave emission originates in the acceleration region directly**.

- These acceleration regions are characterized by relatively **strong magnetic fields and high densities derived from the GS fits** to the microwave data.

- The high-density coronal loops are known to produce significant X-ray emission. From this perspective, it is striking that ***the thermal number density derived from the thermal part of the HXR fits is an order of magnitude or more smaller*** than that derived from the microwave fits.

- This implies that

i. the microwave and HXR emission come from distinct volumes with different number densities and different magnetic fields,

ii. the denser thermal plasma in the microwave source is colder than that in the thermal HXR source; otherwise, the denser source would dominate the thermal HXR emission, and

iii. the magnetic field is smaller at the soft X-ray source than in the microwave source; otherwise, the volume producing the SXR emission would dominate the radio emission.

- We propose that the radio sources in our sample of the narrowband microwave bursts are at lower heights than the accompanying SXR sources; otherwise, it is difficult to obtain the properties (ii) and (iii) itemized above.

Histograms of the frequency-dependent decay constants

Decay constants not consistent with any of the trapping scenarios

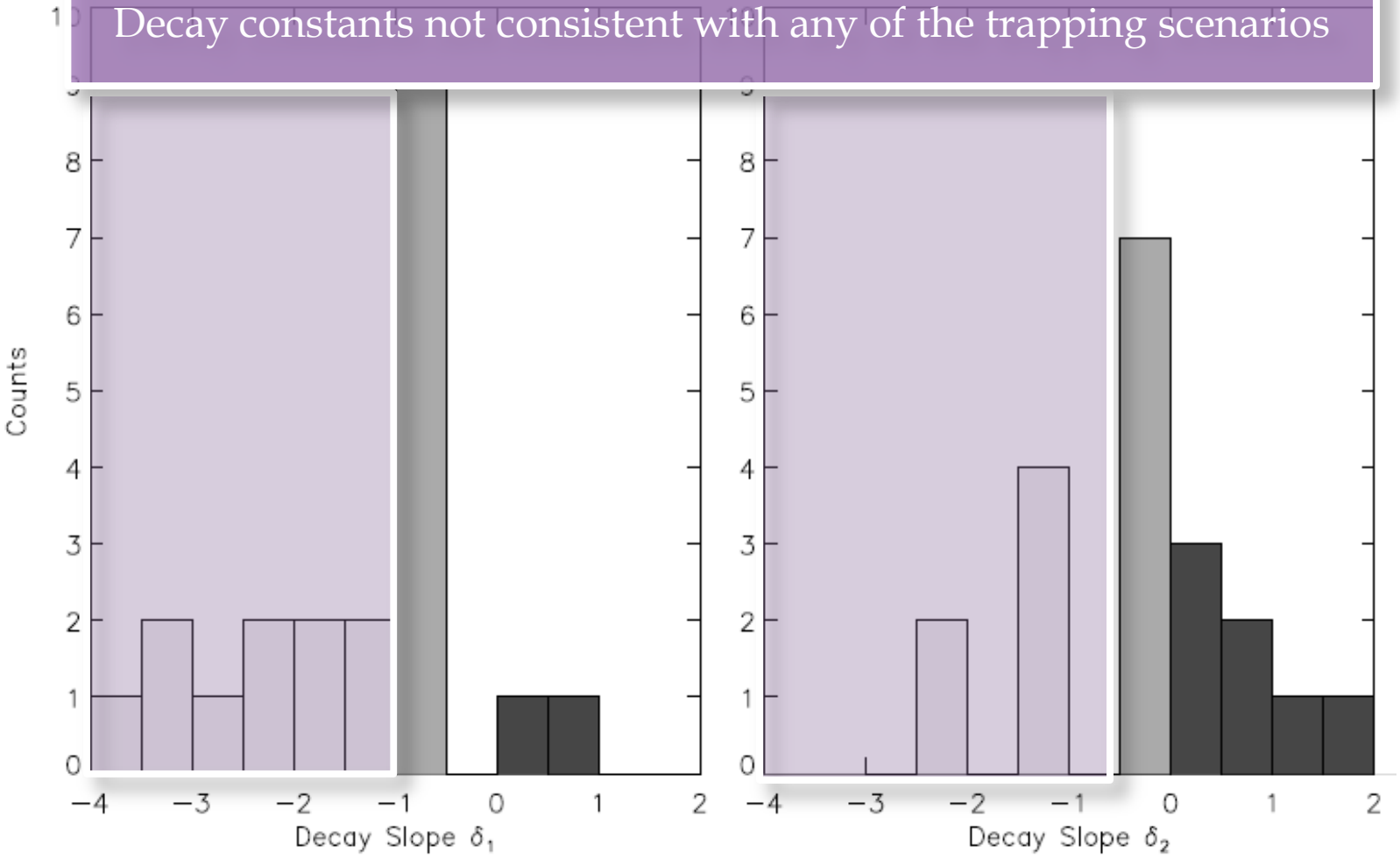

Summary

We identified a new subclass of solar flares, which is characterized by a **narrowband spectrum of microwave emission** that likely comes directly from the **acceleration region**.

The analysis performed implies that energy release in these flares occurred due to **interaction between at least two distinct loops**.

One of the loops is a compact dense loop with a reasonably strong magnetic field, which is observed as a narrowband microwave source, whose physical parameters are determined through the spectral fit.

The other loop is a more tenuous bigger loop, with a smaller magnetic field, which is seen in SXR but barely or not seen in the microwave range.

Study of the detailed morphology of such flares has to await a better quality imaging radio observations.

Thank you!

Extra Slides

Trapping vs acceleration

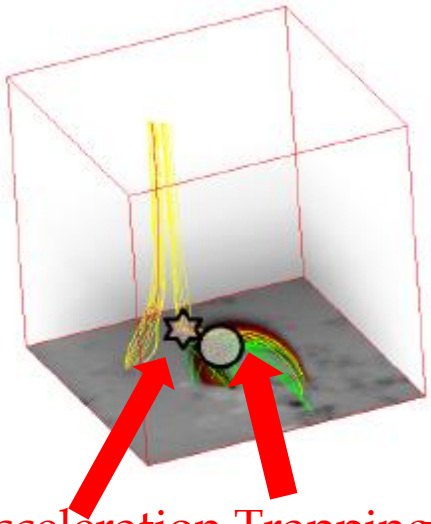

Acceleration Trapping

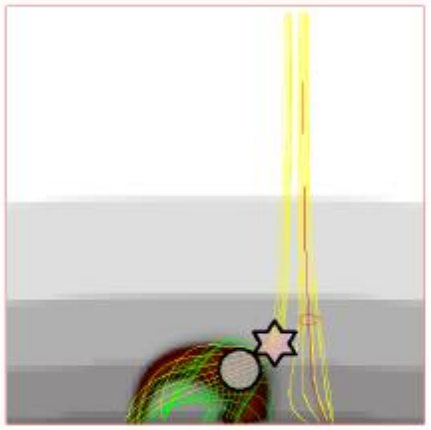

$$\frac{\partial F_A(E,t)}{\partial t} + \hat{L}F_A(E,t) + \frac{F_A(E,t)}{\tau_e(E)} = 0,$$

$$\frac{\partial F_T(E,t)}{\partial t} + \frac{F_T(E,t)}{\tau_T(E)} = Q(E,t)$$

$$F_T(E,t) = \int_{-\infty}^{t} \exp\left(-\frac{t-t'}{\tau_T(E)}\right) Q(E,t')dt'.$$

case of efficient trapping, $\tau_A(E) \ll \tau_T(E)$

$$F_T(E,t) \approx \exp\left(-\frac{t}{\tau_T(E)}\right) \int_{-\infty}^{\infty} Q(E,t')dt',$$

for $t \gg \tau_A$.

Trapping regimes

$$\tau_T(E) \propto E^{\alpha}$$

$$\tau_T(E) \propto \tau_T(f^{1/a}),\ \text{i.e.,}\ \tau_T(E) \propto f^{\alpha/2}$$ for relativistic el's

$$\tau_T(E) \propto \tau_T(f) \propto f^{\alpha/(1-1.5)}$$ For non- or mildly relativistic el's

Moderate diffusion

$$\tau_c \approx 0.95 \cdot 10^8 E_{keV}^{3/2} n_{th}^{-1} (20/\ln\Lambda)$$

$$\tau = mL/v \propto v^{-1}$$

Weak diffusion

$$\tau_{iso} \propto \beta^{1-\nu}\gamma^{2-\nu}$$

$$W_k \propto k^{-\nu}$$

Strong diffusion

$$\tau \sim L^2/\Lambda v \propto \beta^{\nu-3}\gamma^{\nu-2}$$

(1) Regime	(2) $\tau(E)$; nonrel.	(3) δ; nonrel	(4) Range of δ	(5) $\tau(E)$; rel.	(6) δ; rel	(7) Range of δ
Weak diff.; Coulomb	$E^{3/2}$	$\frac{3}{2a}$	$1 < \delta < 3/2$	E^{1}	$1/2$	$1/2$
Weak diff.; Turb.	$E^{(1-\nu)/2}$	$\frac{1-\nu}{2a}$	$-\frac{1}{2} < \delta < 0$	$E^{(2-\nu)}$	$\frac{2-\nu}{2}$	$0 < \delta < \frac{1}{2}$
Moderate diffusion	$E^{-1/2}$	$-\frac{1}{2a}$	$-1/2 < \delta < -1/3$	E^{0}	0	0
Strong diffusion	$E^{(\nu-3)/2}$	$\frac{\nu-3}{2a}$	$-1 < \delta < -\frac{1}{3}$	$E^{(\nu-2)}$	$\frac{\nu-2}{2}$	$-\frac{1}{2} < \delta < 0$

Source morphology

- Perhaps, the simplest model containing two distinct volumes is a flare involving two (interacting) magnetic flux tubes: one of them is the dense loop with a strong magnetic field seen in the microwave emission and identified as the flare acceleration region, while the other one is a more tenuous flux tube with a smaller magnetic field seen in the thermal HXR emission. The presence of more than one loop in many of our events is confirmed by complexity of the HXR source morphology (next slide), which often shows a few distinct sources (footpoints?), especially at the highest energy channel (25–50 keV). In such cases the dominant microwave source should spatially correlate with the high-energy HXR emission. A direct test of this model could be performed based on detailed HXR and microwave image comparison at various energies/frequencies, which could reveal a multi-loop morphology; however, we only have joint *RHESSI* and OVSA imaging data for a few events from the list, so the comprehensive analysis could not be performed.
- For one, relatively strong microwave event of 18-Aug-2002 20:19 UT, conclusive information can be obtained. Next slide shows *RHESSI* 25–50 keV image demonstrating three distinct sources, presumably—footpoints, on which thermal X-ray emission at 9-15 keV is shown in red contours. This low-energy, presumably coronal, source connects two most distant HXR footpoints. On the contrary, the high-frequency (7.4–10.6 GHz) image (white contours) synthesized for the microwave spectral peak range is located between two close southern footpoints, highlighting a smaller coronal loop that produces most of the microwave emission from the flare. The right panel of this plot shows a lower-frequency (6.2–6.6 GHz) source highlighting a bigger loop that connects the most distant footpoints alike the thermal X-ray source. The only viable reason for the displacement between the high- and lowfrequency sources is that the spectrum of the main source dies away quickly at the lower frequency, so the emission from an overall weaker source becomes dominant at reasonably low frequencies. The lower-frequency GS source, which nearly coincides with the thermal X-ray source, implies a weaker magnetic field in that source in full agreement with our interpretation of the data.